Linearly Polarized Emission of an Organic Semiconductor Nanobelt

Aniket Datar,[†] Kaushik Balakrishnan,[†] Xiaomei Yang,[†] Xiaobing Zuo,[‡] Jialing Huang,[§] Randy Oitker,[†] Max Yen,[§] Jincai Zhao,[||] David M. Tiede,*,[‡] and Ling Zang*,[†]

Department of Chemistry and Biochemistry, Southern Illinois University, Carbondale, Illinois 62901, Chemistry Division, Argonne National Laboratory, 9700 South Cass Avenue, Argonne, Illinois 60439, Materials Technology Center (MTC), Southern Illinois University, Carbondale, Illinois 62901, and Key Laboratory of Photochemistry, Institute of Chemistry, Chinese Academy of Sciences, Beijing 100080, China

Received: March 21, 2006; In Final Form: May 2, 2006

Linearly polarized emission has been observed for the nanobelts fabricated from a perylene diimide molecule through both solution-based and surface-supported self-assembling. The measurement of polarized emission was performed over single nanobelts with use of a near-field scanning optical microscope (NSOM) adapted with emission polarization (by putting a planar polarizer before the detector). Rotating the emission polarizer (from 0° to 180°) changed the emission intensity in a way depending on the relative angle between the long axis of the belt and the polarizer with a minimum of intensity detected at ca. 78°, which is indicative of the tilted stacking of molecules along the belt direction.

Introduction

Highly organized materials assembled from organic semiconductor molecules have found enormous applications in optoelectronics. Particularly, the one-dimensional (1D) nanostructures (e.g., nanowires) self-assembled via noncovalent intermolecular interactions have gained increased attention due to their potential application in miniaturization of various optoelectronic devices such as sensors, photovoltaics, and light-emitting diodes.[1,2] Recent evidence suggests that $\pi-\pi$ stacking is an effective way to assemble 1D nanowire structures from rigid, disc-shape aromatic molecules.[3–7] Considering the parallel conformation between packed molecules, the anisotropy in the cross-section plane is expected to be small compared to the anisotropy along the $\pi-\pi$ stacking, i.e., the nanowire thus fabricated is likely uniaxial (along the $\pi-\pi$ stacking direction)[8] in terms of electronic and optical properties. Indeed, the electrical conductivity (charge carrier mobility) of self-assembled organic semiconductors has proven to be most favored by the $\pi-\pi$ stacking.[9] Such a favored conductivity is mainly due to the strong π-electron delocalization (caused by electronic coupling) between the packed molecules.[10–12] However, much less work has been done on the characterization of uniaxial optical properties (such as emission) of the 1D assembly formed by $\pi-\pi$ stacking, although some descent theoretical models have been developed to describe the quantum-confined excitons within quasi-1D organic crystals.[13,14]

The uniaxial optical property coupled with the uniaxial conductivity may lead to a new generation of optical sensors or switches in response to polarized light, which will potentially provide higher selectivity and sensitivity. To this end, there is a great need to investigate the uniaxial optical property of the nanowires self-assembled from $\pi-\pi$ stacking of aromatic molecules. The challenge for the nanoscale exploration is 2-fold: first, to fabricate highly organized nanowires in well-defined morphology (shape and size); second, to perform the measurement at the *single-wire* level (to eliminate the interference of the different orientations of multiple nanowires randomly distributed on surface).

Herein, we report a single-wire investigation of the linearly polarized emission of 1D self-assembly of organic semiconductor molecules, particularly a derivative of perylene tetracarboxylic diimide (PTCDI), a unique class of n-type semiconductor molecules (compared to the more common p-type counterparts) with extremely high thermal stability and photostability,[15] and broad applications in optoelectronics.[16–22] The single-wire measurement of the polarized emission of self-assemblies will likely help reveal the orientation of molecular arrangement, which determines the optical transition dipole of the aggregate. Both experimental and theoretical models have suggested that the optical properties of molecular self-assemblies are strongly dependent on the molecular arrangement within the assembly. Particularly for PTCDI, the electronic transition energy and probability (i.e., the wavelength and intensity of absorption and emission) of the molecular aggregates are dictated by the molecular packing conformation between the component molecules.[23–25] Depending on the interference of side-chain interaction, the packing can be deviated from the strictly co-facial conformation to a certain extent due to the longitudinal and/or transverse slippage of molecular planes.

Experimental Section

Materials. *N,N′*-Di(propoxyethyl)perylene-3,4,9,10-tetracarboxylic diimide (PE-PTCDI, molecular structure shown in Figure 3D) was synthesized following the same method described in a previous work.[26] The starting materials and all solvents (HPLC or spectroscopic grade) were purchased from Fisher and Aldrich, and used as received.

Pyrex glass cover slips (from Corning Inc.) were used as the support substrate for both the self-assembly (through solvent–vapor annealing, vide infra) and microscopy investigation of

* Address correspondence to this author. E-mail: (L.Z.) lzang@chem.siu.edu and (D.M.T.) tiede@anl.gov.

† Department of Chemistry and Biochemistry, Southern Illinois University.

‡ Chemistry Division, Argonne National Laboratory.

§ MTC, Southern Illinois University.

|| Institute of Chemistry, Chinese Academy of Sciences.

the nanostructures. Prior to use, a cover slip was cleaned with piranha reagent (30:70 H_2O_2(35%):H_2SO_4), followed by rinsing with water and methanol.[16] *Caution*: *Piranha solution is an extremely strong oxidizing reagent.* The roughness of the glass surface thus cleaned was about 0.8 nm as confirmed by the shear-force mode topography measurement performed with a scanning probe microscope (Aurora III, Veeco). Such a flat surface is suitable for both the surface fabrication and microscopy measurement of the nanobelts, which have a thickness in the range of a few tens of nanometers.

Fabrication of Nanobelts. Nanobelts of PE-PTCDI were fabricated through self-assembly in both solution and solvent vapor. The former was based on a technique called "phase transfer", an improved fabrication technique based on the "direct dispersion" method previously developed in our lab.[26] Briefly, the 1D growth of the molecular assembly was processed through slow crystallization at the interface between a "good" and a "poor" solvent, where the slow "phase transfer" between the two solvents decreases the solubility at the interface. The poor solvent (e.g., methanol) is normally quite different (e.g., in terms of polarity) from the good solvent (e.g., chloroform), thus providing the possibility to keep the two solvents in separate phases for an extended period. Typically, a larger amount (10:1 v/v) of poor solvent was transferred atop a concentrated chloroform solution of PE-PTCDI ($\sim$0.4 mM) in a test tube. Within minutes, red crystals formed at the interface, followed by slow diffusion into the upper phase of methanol. The nanobelts thus formed can be transferred and cast onto a glass surface by pipetting.

Beyond the solution processing, we have developed a solvent−vapor annealing technique for fabricating nanobelts of PE-PTCDI molecules on a glass surface. Such an approach provided us with in situ preparation of nanobelts on glass suited for microscopy investigation. The annealing was performed in a desiccator having a lid with a valve-controlled vent, which was connected to a vacuum pump. About 30 mL of solvent in a beaker was put in the chamber, followed by vacuum pumping for about 5 min. The chamber was then sealed by closing the vent, leading to saturation of the solvent vapor inside the chamber. The sample was kept in the vapor environment for an extended period (normally 12 to 24 h) to complete the annealing process. The sample, typically a thin film on glass, was prepared by spin-coating of a concentrated chloroform solution of PE-PTCDI ($\sim$0.4 mM) at a speed of 1500 rpm.

General Spectroscopy and Microscopy Characterization. The fluorescence spectra of PE-PTCDI nanobelts were recorded with a modular fluorometer (Photon Technology International Inc.), which allows for highly sensitive measurement of the low emission of solid state PE-PTCDI. The small-angle X-ray diffraction was carried out using the undulator beam line 12-ID at Advanced Photon Source (APS), Argonne National Laboratory, where the instrument is equipped with a double-crystal Si(111) monochromator and a two-dimensional mosaic CCD detector. The X-ray wavelength is normally set at $\lambda =$ 1.0 Å and the sample to detector distance can be adjusted to achieve scattering measured across the range of momentum transfer 0.02 Å^{-1} < q < 3.0 Å^{-1}, where $q = (4\pi/\lambda) \sin \theta$, and λ is the X-ray wavelength and 2θ is the scattering angle. The sample used for X-ray diffraction measurement was prepared by depositing the nanobelts fabricated in methanol onto the surface of Kapton film. The diffraction background was corrected with the blank Kapton film. The fluorescence microscopy imaging was carried out with a Leitz Orthoplan II microscope equipped with a real-color CCD camera for catching

SCHEME 1: The Basic Working Principle of the NSOM Used in This Study[a]
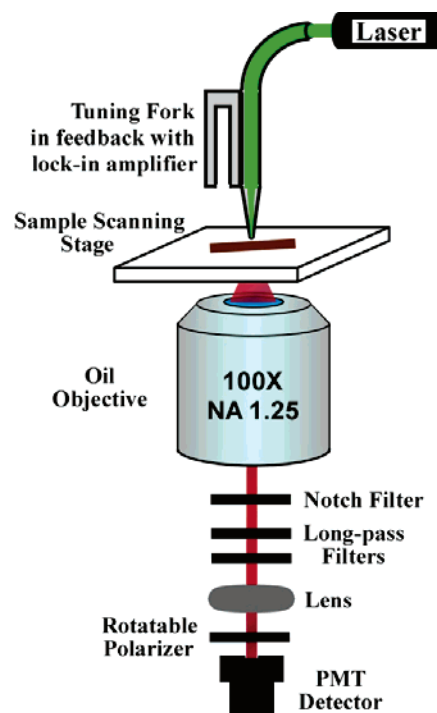
[a] Linear polarized laser is used as the excitation source. A notch filter is used for blocking the excitation beam at 488 nm.

the emission image. Two filter sets were available for exciting the sample at different wavelength regions: the FITC filter set with excitation at 450−490 nm and emission collected at >515 nm, and the Rhodamine filter set with excitation at 530−560 nm and emission collected at >580 nm. The AFM measurement was carried out in tapping mode on a TopoMetrix Explorer, using an antimony doped silicon tip. The largest scanning area is 50×50 μm^2, and the highest z-resolution is about 0.2 nm. The samples were prepared by casting the nanobelt suspension on a mica or glass surface, followed by drying in air for 1−2 h.

NSOM Imaging of a Single Nanobelt. The NSOM system used in this study was set up mainly based on the prototype NSOM obtained from Veeco (Aurora III, see Scheme 1). The central part of NSOM is the tapered, aluminum-coated, single-mode optical fiber probe (Veeco, model 1640-00), which is ended with a tiny aperture of 50−80 nm. High optical resolution is achieved by illuminating a sample through the subwavelength aperture while the sample is held in close proximity (namely the near-field region) to the probe. Within the near-field region the optical resolution is limited only by the probe aperture size, breaking the diffraction limit (λ/2) to the resolution of an ordinary optical microscopy. The NSOM tip−sample distance is regulated by feedback mechanisms similar to those used in AFM. Simultaneous high-resolution optical (50−80 nm) and topographical ($\sim$10 nm x,y-resolution, $\sim$0.2 nm z-resolution) images were obtained by raster scanning over the sample. Thus, with NSOM the spectral properties (e.g., emission intensity) of a nanobelt can be directly correlated to the topography features (e.g., size and shape).

Results and Discussion

As previously proven, self-assembly of PE-PTCDI molecules produces well-defined one-dimensional nanostructures, mainly due to the minimal steric hindrance of the short, linear side
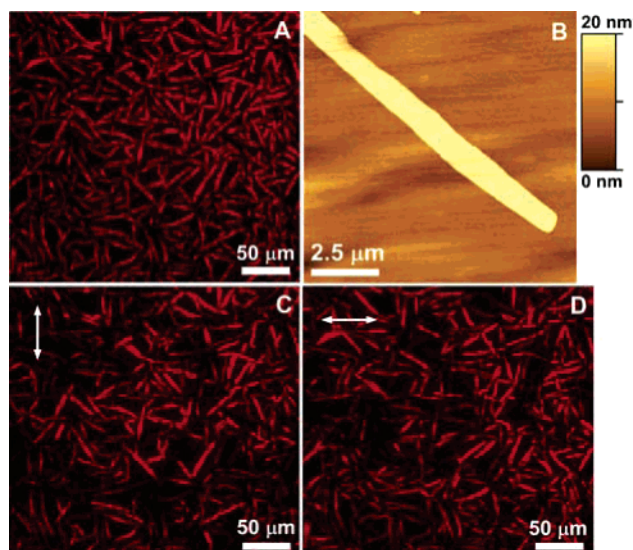
Linearly Polarized Emission of an Organic Nanobelt

J. Phys. Chem. B, Vol. 110, No. 25, 2006 **12329**

Figure 1. (A) fluorescence microscopy images of the nanobelts of PE-PTCDI fabricated in situ on glass via chloroform vapor annealing. Excitation: 450−490 nm; emission collected at >515 nm. (B) AFM image of part of a single nanobelt showing the flat morphology of the belt, with uniform thickness of about 20 nm. (C and D) fluorescence microscopy images of the same area as in part A but with polarized excitation. The direction of the excitation polarization is indicated by the arrow labeled at the top left in each figure.

chains, which are highly cooperative to the $\pi-\pi$ stacking between molecules.[26] Upon being dispersed in a "poor" solvent like methanol, these molecules self-assemble into nanobelt structures. In this study, we have developed an improved technique (e.g., phase-transfer processing) to fabricate the nanobelts suited for discrete dispersion on surface. This new technique also allows for slow crystallization (and thus formation of more extended and uniform belt structure) at the interface between a good and a poor solvent. Beyond the solution processing method, a surface-supported solvent−vapor annealing technique was also developed and employed to fabricate nanobelts in situ on the surface of glass, where the generated nanobelts are sparsely distributed, thus facilitating the microscopy imaging of the polarized emission, which is directly correlated to the orientation of individual nanobelts.

Figure 1A shows a fluorescence microscopy image of the nanobelts of PE-PTCDI fabricated on the glass surface via chloroform vapor annealing (24 h). The uniform intensity observed over a large area of sample suggests a well-defined morphology (e.g., size and shape) of the nanobelts. An AFM image zoomed onto a single fiber showed clearly a belt configuration with flat surface and thickness of only about 20 nm (Figure 1B), which indicates an aspect ratio (length over thickness) larger than 2500. The emission depicted in Figure 1A was obtained with excitation at 450−490 nm, at which both the individual molecules and the crystal phase of PTCDI could be excited (Figure 2). However, the emission observed is predominantly from the crystalline phase as revealed by the red color. This implies that the strong intermolecular interactions lead to formation of organized materials with collective electronic structures that are different from those of the individual component molecules (which emit in the green region). With excitation at longer wavelengths (530−560 nm), at which mainly the crystalline phase is excited, the emission color (wavelength) was found to be the same as observed at a excitation of shorter wavelength, further implying that the emission of the assembled crystal was only from the lowest
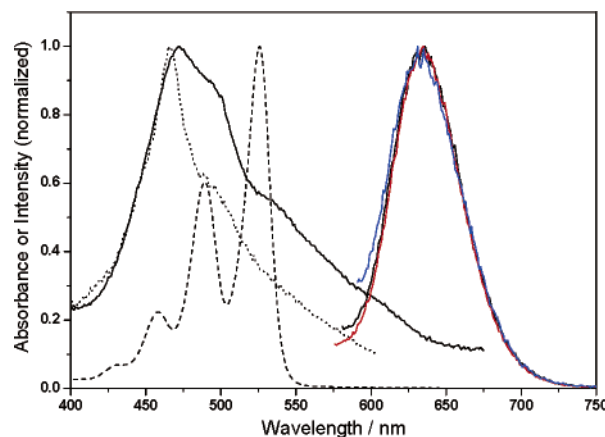

Figure 2. (Left) UV−vis absorption spectrum (solid line) and fluorescence excitation spectrum (dotted line, $\lambda_{em} = 635$ nm) of the PE-PTCDI aggregate spin-cast on glass. (Right) The fluorescence emission spectra recorded at different excitation wavelengths: 450 (black), 468 (red), and 520 nm (blue). The absorption spectrum of a homogeneous solution of PE-PTCDI in chloroform (1.2 μM) is also shown for comparison.

excimer-like state (which is formed mainly due to the strong electronic coupling between the π-orbitals).[23,27]

The fluorescence microscopy observation was consistent with the UV−vis absorption and fluorescence spectral measurement for the aggregate of PE-PTCDI spin-cast on glass (Figure 2). Regardless of the excitation wavelength (450, 468, 520 nm), the emission spectra demonstrate almost the same shape and center at the same wavelength (λ_{max} 635 nm), confirming that the observed emission is indeed due to the lowest electronic-coupling state formed between the π-stacked molecules. As shown in the excitation spectrum recorded at emission λ_{max} 635 nm, the electronic transition from the ground state to the higher energy π-stacking state ($\sim$465 nm) is predominant over the transition to the lower energy state (at longer wavelength), consistent with the previous observation on other PTCDI molecules.[27] Compared to the excitation spectrum, the absorption spectrum of the PE-PTCDI aggregate shows relatively higher intensity at the longer wavelengths. Such a discrepancy was previously observed for the aggregate of other PTCDIs.[28] The decreased emission at excitation of longer wavelength is (although not yet clear) likely due to the unfavorable transition from the excimer-like (lower energy) state to the ground state.[4] Such an emitting transition generally demands a structural alteration of the excimer-like state, which in turn requires extra excited-state energy (that can be provided by excitation at shorter wavelength).

1D self-assembly of PTCDI-like molecules usually depicts optically uniaxial property along the $\pi-\pi$ interaction.[8] This is reminiscent of the uniaxial columnar packing of discotic liquid crystal molecules, providing an option of using polarized emission spectrometry to characterize the molecular packing conformation. Particularly, such measurement can be performed under a fluorescence microscope with a polarized excitation beam, with which the sparsely dispersed nanobelts can be separately excited depending on the different orientation. Panels C and D of Figure 1 show the emission images of the PE-PTCDI nanobelts collected under polarized excitation with the polarizer positioned vertically and horizontally, respectively. Clearly, the two figures are complementary to each other in term of emission intensity of individual nanobelts, i.e., some nanobelts show diminished emission at vertically polarized excitation, while the others show the same diminishing at horizontally polarized excitation. This observation indicates that the transition dipole

moments of the emission state of different nanobelts are oriented at different directions as the nanobelts are randomly distributed on the surface. For a single nanobelt, the polarization dependence of the emission intensity appears to be the same for the whole fiber (as inferred from the uniform intensity observed), implying that the molecular packing conformation (crystalline structure) for a given nanobelt is consistent along the whole fibril phase. This is consistent with our recent observation of the birefringence of single-nanobelts under a cross-polarized microscope.[26]

As previously observed for the bulk crystals of PTCDI and the analogues,[8,24,25] the component molecules within a nanobelt are expected to pack parallel, and tilt at an appropriate angle with respect to the long axis of the belt. The tilted, parallel packing conformation resembles the slipped H-aggregate for the imaging dyes (cyanines) and other aromatic chromophores such as porphyrins.[3] The tilted angle is mainly dependent on the molecular configuration and the side-chain structure.[25] Within a single nanobelt, the molecules are packed parallel to each other. However, if there are multiple nanobelts under measurement, the belts may be aligned in different directions on a surface, and thus the orientation of transition dipole moments (due to the $\pi-\pi$ electronic coupling of the molecules) becomes different for different nanobelts. For example, parallel alignment of a pair of nanobelts on a surface does not mean the component molecules in the two belts are necessarily parallel to each other. To this end, studying the polarized emission of the nanobelts (in correlation to the molecular packing) requires a measurement on *a single-belt*, which in turn requires a high-resolution optical microscopy technique. An ordinary far-field optical microscope can hardly focus (zoom) on a single nanowire or belt with a submicron width, mainly due to the diffraction limit.

In this work, we used NSOM to image the single nanobelt by exciting the nanobelt in near-field and recording the fluorescence in far-field. Such a microscopy system allows for convenient adjustment of the polarization of the emission recording (Scheme 1). Within the near-field the optical resolution of NSOM is limited only by the probe aperture size (∼50 nm), thus breaking the diffraction limit to the resolution of ordinary optical microscopy. Moreover, NSOM measurement provides direct correlation between the nanoscale topography information (e.g., size, thickness, and orientation) and the optical property (e.g., emission) of a nanobelt.[29] Such a correlated measurement is crucial for evaluating the polarization property of molecular self-assemblies.

Coupled with the far-field polarization modulation of the emission, NSOM provides an essential approach to characterizing the local molecular orientation of samples, leading to a global 2D mapping of the homogeneity of the molecular packing conformation. The optical resolution (∼50 nm) offered by the NSOM probe is high enough to laterally image the nanobelt fabricated in this study, which is a few hundreds of nanometers in width and a few tens of microns in length. In case a nanobelt is composed of randomly oriented poly-nanocrystalline domains, the distribution of such domains can be revealed by measuring the emission polarization via raster scanning the surface with the NSOM probe. In contrast, such randomly aligned nanocrystals can hardly be detected by ensemble measurement with ordinary optical microscopes, because the difference in emission intensity due to polarization modulation is averaged out by simultaneously measuring a large number of nanocrystals that could be oriented at all the possible directions.
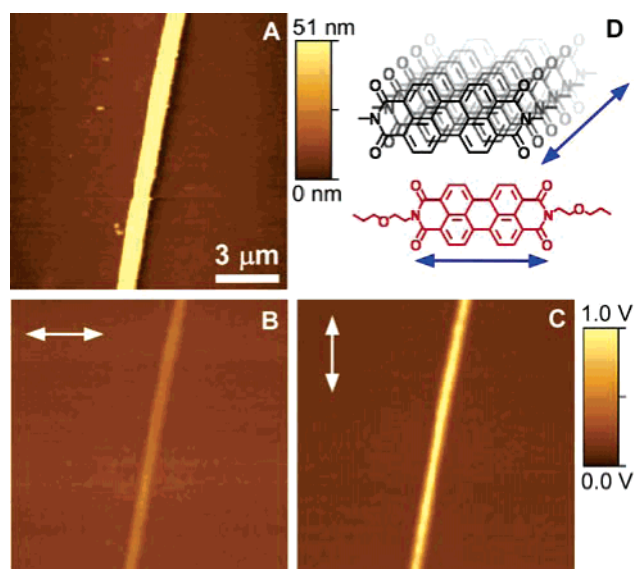

Figure 3. (A) NSOM topography image of a nanobelt assembled from PE-PTCDI using the "phase transfer" method; belt thickness is about 50 nm, and the width is about 1.0 μm. (B and C) NSOM emission images collected (by PMT) after a polarizer is placed at horizontal and vertical positions, respectively. The polarization of the excitation laser (488 nm, Ar$^+$) is horizontal in the image, and the polarization purity is larger than 250:1. (D) Schematic diagram showing the $\pi-\pi$ stacking of PE-PTCDI molecules: blue arrows indicate the transition dipole of an individual PTCDI molecule and the $\pi-\pi$ stacked aggregate. The offset of molecular stacking is omitted for clarity.

Figure 3A shows a nanobelt imaged by topography scanning with NSOM. This specific nanobelt was highly uniform in both thickness (∼50 nm) and width (∼1.0 μm). Emission detected within the same raster-scanning showed uniform intensity along the whole belt (data not shown), consistent with the homogeneous thickness of the nanobelt. Putting a planar polarizer before the emission detector (a PMT) changed the emission intensity depending on the polarizer angle with respect to the orientation of the nanobelt. With the polarizer positioned close-to-perpendicular to the long axis of the belt, the emission was diminished (Figure 3B), while at a position close-to-parallel to the nanobelt, the emission was enhanced (Figure 3C). These results imply that the transition dipole moment to the lowest excitonic state of the molecular assembly is oriented approximately along the long axis of the nanobelt (i.e., the direction of $\pi-\pi$ stacking). The transition dipole of the π-stacked molecular aggregate is likely perpendicular to the molecular plane of PTCDI, while the transition dipole of an individual molecule is completely in plane, along the N−N axis (Figure 3D).[23,24] Such a dramatic reorientation of transition dipole moment has also been observed for the $\pi-\pi$ stacked dimers of aromatic molecules (e.g., phenalene),[10] for which the orientation of electronic transition dipole changes from in-plane (for an individual molecule) to perpendicular to the molecular plane (for the dimer).

Consequently rotating the emission polarizer changed the emission intensity in an alternate way depending on the relative angle (0−180°) between the long axis of the belt and the polarizer, with a minimum of intensity detected at ca. 78° (Figure 4), which is indicative of the tilted molecular stacking along the belt direction. The maximal intensity ($I_{\parallel}$, intensity measured with emission polarizer parallel to the dipole moment of nanobelt) thus detected was about 7.5 times higher than the minimal intensity ($I_{\perp}$, intensity measured with emission polarizer perpendicular to the dipole moment of the nanobelt). On the basis of this maximal/minimal intensity ratio ($I_{\parallel}/I_{\perp}$), one can

Linearly Polarized Emission of an Organic Nanobelt

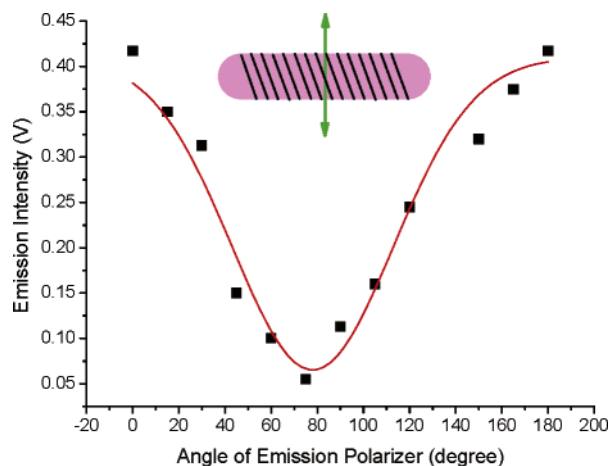*J. Phys. Chem. B, Vol. 110, No. 25, 2006* **12331**

Figure 4. Emission intensity of a single PE-PTCDI nanobelt depending on the angle between the polarizer and the long axis of the nanobelt. The inset (cartoon) shows the tilted packing of molecules along the long axis of the nanobelt, which is aligned at 90° to the polarizer (marked as an arrow). The emission transition dipole of the molecular stacking is assumed to be perpendicular to the molecular plane. Measurement over several nanobelts showed similar behavior as depicted in this figure.

calculate the polarization factor, $(I_{||} - I_{\perp})/(I_{||} + I_{\perp})$, to be about 75%. Such a large value is quite close to that obtained for the single-crystalline CdSe nanorods (a highly fluorescent inorganic semiconductor),[30] which was reported to be highly linearly polarized in emission.

It should be noted that the data shown in Figure 4 were based on the measurement of one specific nanobelt. To ensure a reliable measurement of the intensity modulation along the whole belt, for each polarizer angle we raster scanned a large area to globally image the emission intensity of a large part of the nanobelt, and used the averaged intensity represented by a line-scan along the long axis of the nanobelt, rather than a pixel intensity, to plot Figure 4. Such measurements took a long time, and could cost multiple NSOM probes (which are fragile), thereby we finished up with no more than four nanobelts (from the same batch sample) for the polarization measurement as depicted in Figure 4. Among the four nanobelts, one showed a globally flat surface and uniform thickness, producing a quite flat intensity line-scan along the belt, thus enabling easy averaging of the intensity over the entire belt. The data shown in Figure 4 were based the measurement of this specific nanobelt.

The tilted molecular packing is partially the result of the molecular interaction between side chains. Depending on the structure of the side chains, different extents of stacking offset (i.e., longitudinal and transverse shift) have been observed for PTCDI molecules, leading to formation of crystal structures with $\pi-\pi$ stacking deviated from the co-facial conformation.[23,24,31] Figure 5 shows the small-angle X-ray diffraction pattern measured for the PE-PTCDI nanobelts deposited on Kapton film. Three major peaks were observed, corresponding to *d* spacing of 16.45, 8.19, and 7.29 Å. The first and third values are correlated to the edge-to-edge distances between two adjacent PTCDI molecules at the longitudinal and transverse directions, respectively, while the second peak is likely due to the secondary diffraction (002) since the *d* spacing is about half of the value of the primary diffraction peak (001). The longitudinal *d* spacing is about 35% shorter than the total length of the PE-PTCDI molecule (including the side chains), 25.43 Å, which was obtained from the energy-optimized conformation of the molecule (DFT calculation with Gaussian 03,[32] B3LYP/6-311g**//
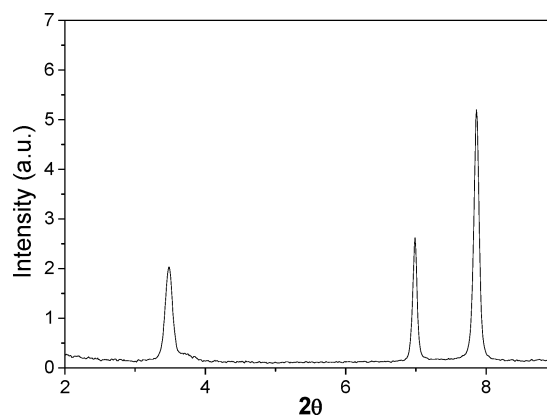

Figure 5. Small-angle X-ray diffraction pattern of the nanobelts assembled from PE-PTCDI.

6-31g*). This implies that about 66% of the propoxyethyl side chains are interdigitated to each other. Such a significant side chain interdigitation has been observed previously for other PTCDI molecules with linear side chains.[24] To "counterbalance" the strong side chain interaction, the PTCDI plane has to be shifted to minimize the total energy of the molecular aggregate,[23] producing a tilted geometry of molecular stacking as observed by the single-belt measurement of the polarized emission (Figure 4).

Conclusion

The linearly polarized emission within a single PTCDI nanobelt has successfully been imaged under near-field excitation. The emission dipole moment was measured at a direction deviating from the long axis of the nanobelt, implying a slightly tilted molecular stacking with respect to the 1D growing direction of the nanobelt. The linear compression of emission makes the 1D nanomaterials potentially ideal for many orientation-sensitive applications, such as polarized light emitting diodes and flat panel displays.

References and Notes

(1) Schenning, A. P. H. J.; Meijer, E. W. *Chem. Commun.* **2005**, 3245.
(2) Grimsdale, A. C.; Mullen, K. *Angew. Chem.*, *Int. Ed.* **2005**, *44*, 5592.
(3) Hoeben, F. J. M.; Jonkheijm, P.; Meijer, E. W.; Schenning, A. P. H. J. *Chem. Rev.* **2005**, *105*, 1491.
(4) Wurthner, F. *Chem. Commun.* **2004**, 1564.
(5) Nguyen, T.-Q.; Martel, R.; Avouris, P.; Bushey, M. L.; Brus, L.; Nuckolls, C. *J. Am. Chem. Soc.* **2004**, *126*, 5234.
(6) Kastler, M.; Pisula, W.; Wasserfallen, D.; Pakula, T.; Mullen, K. *J. Am. Chem. Soc.* **2005**, *127*, 4286.
(7) Hill, J. P.; Jin, W.; Kosaka, A.; Fukushima, T.; Ichihara, H.; Shimomura, T.; Ito, K.; Hashizume, T.; Ishii, N.; Aida, T. *Science* **2004**, *304*, 1481.
(8) Friedrich, M.; Wagner, T.; Salvan, G.; Park, S.; Kampen, T. U.; Zahn, D. R. T. *Appl. Phys. A* **2002**, *75*, 501.
(9) Guillon, D. *Struct. Bonding* **1999**, *95*, 41.
(10) Small, D.; Zaitsev, V.; Jung, Y.; Rosokha, S. V.; Head-Gordon, M.; Kochi, J. K. *J. Am. Chem. Soc.* **2004**, *126*, 13850.

(11) Crispin, X.; Cornil, J.; Friedlein, R.; Okudaira, K. K.; Lemaur, V.; Crispin, A.; Kestemont, G.; Lehmann, M.; Fahlman, M.; Lazzaroni, R.; Geerts, Y.; Wendin, G.; Ueno, N.; Bredas, J.-L.; Salaneck, W. R. *J. Am. Chem. Soc.* **2004**, *126*, 11889.

(12) Rochefort, A.; Martel, R.; Avouris, P. *Nano Lett.* **2002**, *2*, 877.

(13) Schmidt, K. *Phys. Lett. A* **2002**, *293*, 83.

(14) Hoffmann, M.; Schmidt, K.; Fritz, T.; Hasche, T.; Agranovich, V. M.; Leo, K. *Chem. Phys.* **2000**, *258*, 73.

(15) Newman, C. R.; Frisbie, C. D.; da Silva Filho, D. A.; Bredas, J.-L.; Ewbank, P. C.; Mann, K. R. *Chem. Mater.* **2004**, *16*, 4436.

(16) Zang, L.; Liu, R.; Holman, M. W.; Nguyen, K. T.; Adams, D. M. *J. Am. Chem. Soc.* **2002**, *124*, 10640.

(17) Holman, M. W.; Liu, R.; Zang, L.; Yan, P.; DiBenedetto, S. A.; Bowers, R. D.; Adams, D. M. *J. Am. Chem. Soc.* **2004**, *126*, 16126.

(18) Xu, B. Q.; Xiao, X.; Yang, X.; Zang, L.; Tao, N. J. *J. Am. Chem. Soc.* **2005**, *127*, 2386.

(19) Li, X.; Xu, B. Q.; Xiao, X.; Yang, X.; Zang, L.; Tao, N. J. *Faraday Discuss.* **2006**, *131*, 111.

(20) Schmidt-Mende, L.; Fechtenkotter, A.; Mullen, K.; Moons, E.; Friend, R. H.; MacKenzie, J. D. *Science* **2001**, *293*, 1119.

(21) Forrest, S. R. *Chem. Rev.* **1997**, *97*, 1793.

(22) Law, K.-Y. *Chem. Rev.* **1993**, *93*, 449.

(23) Kazmaier, P. M.; Hoffmann, R. *J. Am. Chem. Soc.* **1994**, *116*, 9684.

(24) Struijk, C. W.; Sieval, A. B.; Dakhorst, J. E. J.; van Dijk, M.; Kimkes, P.; Koehorst, R. B. M.; Donker, H.; Schaafsma, T. J.; Picken, S. J.; van de Craats, A. M.; Warman, J. M.; Zuihof, H.; Sudholter, E. J. R. *J. Am. Chem. Soc.* **2000**, *122*, 11057.

(25) Klebe, G.; Graser, F.; Hadicke, E.; Berndt, J. *Acta Crystallogr.* **1989**, *B45*, 69.

(26) Balakrishnan, K.; Datar, A.; Oitker, R.; Chen, H.; Zuo, J.; Zang, L. *J. Am. Chem. Soc.* **2005**, *127*, 10496.

(27) Ahrens, M. J.; Sinks, L. E.; Rybtchinski, B.; Liu, W.; Jones, B. A.; Giaimo, J. M.; Gusev, A. V.; Goshe, A. J.; Tiede, D. M.; Wasielewski, M. R. *J. Am. Chem. Soc.* **2004**, *126*, 8284.

(28) Gregg, B. A. *J. Phys. Chem.* **1996**, *100*, 852.

(29) Vanden Bout, D. A.; Kerimo, J.; Higgins, D. A.; Barbara, P. F. *Acc. Chem. Res.* **1997**, *30*, 204.

(30) Hu, J.; Li, L.-S.; Yang, W.; Manna, L.; Wang, L.-W.; Alivisatos, A. P. *Science* **2001**, *292*, 2060.

(31) Hadicke, E. H.; Graser, F. *Acta Crystallogr.* **1986**, *C42*, 189.

(32) Frisch, M. J.; Trucks, G. W.; Schlegel, H. B.; Scuseria, G. E.; Robb, M. A.; Cheeseman, J. R.; Montgomery, J. A., Jr.; Vreven, T.; Kudin, K. N.; Burant, J. C.; Millam, J. M.; Iyengar, S. S.; Tomasi, J.; Barone, V.; Mennucci, B.; Cossi, M.; Scalmani, G.; Rega, N.; Petersson, G. A.; Nakatsuji, H.; Hada, M.; Ehara, M.; Toyota, K.; Fukuda, R.; Hasegawa, J.; Ishida, M.; Nakajima, T.; Honda, Y.; Kitao, O.; Nakai, H.; Klene, M.; Li, X.; Knox, J. E.; Hratchian, H. P.; Cross, J. B.; Bakken, V.; Adamo, C.; Jaramillo, J.; Gomperts, R.; Stratmann, R. E.; Yazyev, O.; Austin, A. J.; Cammi, R.; Pomelli, C.; Ochterski, J. W.; Ayala, P. Y.; Morokuma, K.; Voth, G. A.; Salvador, P.; Dannenberg, J. J.; Zakrzewski, V. G.; Dapprich, S.; Daniels, A. D.; Strain, M. C.; Farkas, O.; Malick, D. K.; Rabuck, A. D.; Raghavachari, K.; Foresman, J. B.; Ortiz, J. V.; Cui, Q.; Baboul, A. G.; Clifford, S.; Cioslowski, J.; Stefanov, B. B.; Liu, G.; Liashenko, A.; Piskorz, P.; Komaromi, I.; Martin, R. L.; Fox, D. J.; Keith, T.; Al-Laham, M. A.; Peng, C. Y.; Nanayakkara, A.; Challacombe, M.; Gill, P. M. W.; Johnson, B.; Chen, W.; Wong, M. W.; Gonzalez, C.; Pople, J. A. *Gaussian 03*; Gaussian: Pittsburgh, PA, 2003.